Single amino acid bionanozyme for environmental remediation

Pandeeswar Makam
Tel Aviv University https://orcid.org/0000-0003-1114-8089
Sharma Yamijala
University of California, Riverside
Linda Shimon
Weizmann Institute https://orcid.org/0000-0002-7861-9247
Bryan Wong
University of California, Riverside https://orcid.org/0000-0002-3477-8043
Ehud Gazit (ehudg@post.tau.ac.il)
Tel Aviv University https://orcid.org/0000-0001-5764-1720

Article

Keywords: minimalistic biomolecular nanomaterials, single amino acid bionanozyme, environmental remediation

Posted Date: August 24th, 2020

DOI: https://doi.org/10.21203/rs.3.rs-61912/v1

Version of Record: A version of this preprint was published at Nature Communications on March 21st, 2022. See the published version at https://doi.org/10.1038/s41467-022-28942-0.

Abstract

Enzymes are extremely complex catalytic structures with immense biological and technological importance. Nevertheless, their widespread environmental implementation faces several challenges, including high production costs, low operational stability, and intricate recovery and reusability. Therefore, the *de novo* design of minimalistic biomolecular nanomaterials that can efficiently mimic the biocatalytic function (bionanozyme) and overcome the limitations of natural enzymes is a key goal in biomolecular engineering. Here, we report an exceptionally simple yet highly active and robust single amino acid bionanozyme that can catalyze the rapid oxidation of environmentally toxic phenolic contaminates and serves as an ultrasensitive tool to detect biologically important neurotransmitters, similar to the laccase enzyme. While inspired by the laccase catalytic site, the substantially simpler copper-coordinated bionanozyme is ∼5400-fold more cost-effective, 10-fold more efficient, and 36-fold more sensitive compared to the natural protein. Furthermore, the designed mimic is stable under extreme conditions (pH, ionic strength, temperature, storage time), markedly reusable for several cycles and display broad substrate specificity. These findings hold great promise in the development of efficient bionanozyme for analytical chemistry, environmental protection, and biotechnology.

Introduction

Over billions of years, enzymes naturally evolved to efficiently catalyze various thermodynamically challenging biochemical reactions, that are necessary to sustain life under physiological conditions.[1] Nonetheless, the exact evolutionary pathway from the simple amino acid building blocks to complex enzyme structures is still enigmatic[2−4]. Enzymes also serve as very useful biocatalysts in several industrial processes owing to their numerous advantages over conventional organic or inorganic catalysts, including milder reaction conditions, exceptional selectivity, and lower environmental and physiological toxicity[5−8]. Many oxidative enzymes have been described that could potentially transform many environmentally toxic compounds into less harmful products[9,10]. Among these, laccases are multicopper-containing oxidases commonly found in bacteria, fungi, plants, and insects that have raised much interest in both fundamental and applied research[11]. These enzymes catalyze the oxidation of a wide array of environmentally toxic phenolic contaminates into unstable phenoxy radical intermediates that further self-couple to form benign polymeric substances, thus underlying laccase use in biotechnology and environmental remediation (Fig. 1a)[12]. Unlike other oxidase enzymes, which require or produce hydrogen peroxide, laccase utilizes only molecular oxygen as the final electron acceptor and releases water as a by-product, with the copper redox ($Cu^{2+/}Cu^{1+}$) reactivity playing a critical role in shuttling the electrons from substrates to oxygen. Hence, laccases are considered eco-friendly, versatile biocatalysts that bear an enormous potential for industrial wastewater treatment. Although laccases are very promising, several intrinsic drawbacks, including high costs of preparation and purification, low operational stability, the sensitivity of catalytic activity to environmental conditions, and inefficient recycling and reusing, severely hamper its widespread in vitro applications.

One of the promising approaches to overcome the limitations of applying natural enzymes in industrial settings is to utilize the enzyme-mimicking nanomaterials, termed nanozymes[13,14]. The concept of nanozymes has emerged as the next generation of enzyme mimics as it links nanomaterials to biological systems and their functions[15]. Compared to natural enzymes, nanozymes are much more cost-effective for production and more robust for diverse applications. Consequently, numerous classes of nanomaterials, including metal oxide nanoparticles, metal nanoparticles, transition metal chalcogenides, alloy nanomaterials, carbon-based nanomaterials, graphene quantum dots, carbon nitride nanomaterials, and metal-organic frameworks, have been discovered to possess unique enzyme-mimetic catalytic activities [14,16–18]. However, it should be noted that most of these materials do not share any common properties or structures of the native enzymes and suffer from harsh synthesis conditions, complicated fabrication steps, the requirement of sophisticated equipment, and time-consuming and hard-templating methods, thus greatly impeding their use in industrial-scale applications. In this regard, peptide-based nanomaterials have attracted growing attention due to their protein-derived nature, ease of large-scale synthesis, and good biodegradability[19–21]. In the past few years, the minimalist approach originally described by DeGrado as “sequences that are simpler than their natural counterparts but, nevertheless, retain sufficient complexity for folding and function” has materialized in the construction of simple biomolecular nanozymes (bionanozymes)[2,22,31–34,23–30]. Despite many efforts, the *de novo* design and development of laccase mimicking bionanozymes is still in its infancy owing to the complex structure of the laccase active site and the complicated catalytic reaction mechanism.

Moving more minimalistic, in this report, we explored whether the self-assembly of a single amino acid can produce a laccase-mimicking bionanozyme for environmental remediation. Inspired by the laccase catalytic active site, we explore the supramolecular assembly of the single amino acid phenylalanine (F) in combination with redox-active divalent copper ions (Cu^{2+}). Among the pool of amino acids, F is an excellent self-assembling structural unit containing metal-chelating amino and carboxylate functionalities., Therefore, it acts as a multidentate ligand to coordinate with the divalent Cu^{2+} [35,36]. The envisioned supramolecular organization of F in the presence of Cu^{2+} is shown in Fig. 1b, where F coordinates with Cu^{2+} to form a novel two-dimensional (2D) layered structures that stacked together through aromatic interactions (F-Cu). The relatively weak van der Waals interlayer interactions facilitate their mechanical exfoliation into either monolayers or several layer thick F-Cu nanosheets. The ultrathin 2D nanosheets coupled with highly accessible crystalline 2D arrays of redox Cu^{2+}/Cu^{1+} ions are anticipated to exhibit an enhanced laccase mimicking catalytic oxidation of toxic phenolic compounds with striking stability. Therefore, this new single-amino-acid bionanozyme approach represents a potential alternative to both protein engineering and other conventional nanozyme approaches. The later procedures are not only time-consuming and chemically challenging but often require expensive experimental setups, harsh reaction conditions, and complex fabrication steps.

Results And Discussion

Synthesis and structural analysis of F–Cu bionanozyme

Mixing of Cu^{2+} with F alkaline solution under mild heating conditions resulted in the formation of blue-colored F-Cu 2D plate-like crystals, which were analyzed using single-crystal X-ray crystallography. The coordination of Cu^{2+} with F, shown in Fig. 2, was octahedral with tetragonal distortion. Two F molecules complexed with one Cu^{2+} through an O (carboxylate), N (amine)-chelating modes, forming two five-membered phenylalanate-Cu^{2+} chelate rings (Fig. 2a). The two aromatic phenyl rings on either side of the chelating rings were in a trans conformation with respect to each other. These primary coordination spheres were further linked together by the second oxygen atom of the carboxylate groups of both F molecules and thus formed an infinite in-plane material strongly coordinated covalent 2D sheet along the crystallographic *a* and *b*-axis (Fig. 2b and 2c). Further, these atom-thin 2D sheets stacked into a layer by layer assembly held together through relatively weak interlayer van der Waals forces (Fig. 2d). To estimate the growth rate of F-Cu 2D layered crystals, we monitored an *in-situ* crystallization process using optical microscopy. Briefly, a quartz cuvette (10 mm) was filled with a freshly prepared alkaline solution of F and mixed with $CuCl_2$ at a 2:1 molar ratio and immediately capped to prevent evaporation or concentration changes. The crystallization process inside the cuvette was monitored under a light microscope at two-second intervals (Supplementary Movie S1). In solution, small nucleation seeds appeared within a few seconds (~28 sec) and laterally extended into large two-dimensional free-standing crystals. A selected single-crystal elongation growth was plotted as a function of time and indicated an estimated elongation rate of 0.5 nms^{-1} at a linear regime (Fig. 2e, Supplementary Movie S2), revealing a spontaneous crystallization process. The corresponding snapshots of three consecutive images at different time points during the crystal growth are shown in Fig. 2e. These F-Cu crystals were further analyzed by high-resolution scanning electron microscopy (HRSEM) and atomic force microscopy (AFM). HRSEM micrographs showed laterally-extended rectangular 2D sheets with 10–500 μm lateral dimensions and layered hierarchy within each 2D crystal (Supplementary Fig S1). AFM topographical measurements showed 260 nm thick 2D crystals composed of several stacks of much thinner 10–20 nm nanolayers (Fig. 2g). Furthermore, owing to the week interlayer van der Waals interactions, the thicker sheets could be readily exfoliated into thinner 2D nanosheets with the assistance of external mechanical shear forces triggered by mild ultrasonication. The AFM topography images after ultrasonication treatment displayed ultrathin ~1.8 nm nanosheets, each comprised of a small number of layers (Fig. 2i) inferred to be atomic monolayers based on the estimated thickness of ~1.6 nm deduced from the X-ray crystal structure (Fig. 2d). In addition, the powder X-ray diffraction (PXRD) patterns of the F-Cu nanosheets and microcrystals were well-matched, revealing the intact nature of the highly crystalline 2D nanosheets (Fig. 2j). The UV-visible absorption spectrum of F-Cu nanosheets displayed a new broad 615 nm absorption band in the visible region assigned to the d-d transition specific to the Cu^{2+} complexes with tetragonal distortion owing to the Jahn–Teller effect (Supplementary Fig S2). The Fourier-transform infrared spectrum (FTIR) of F-Cu nanosheets showed a new broad metal-oxygen stretching band at 555 cm^{-1} (ν_{M-O}) and a significant red shifted in ($\Delta\nu$ = 125 cm^{-1}) amine absorption band, suggesting strong in-plane carboxylate- and amine-Cu^{2+} coordination modes (Supplementary Fig S2). Energy

dispersive X-ray (EDX) spectral analysis confirmed the presence of the elemental composition of Cu atoms along with carbon (C) and oxygen (O) within the F-Cu nanosheets (Supplementary Fig S2). Thermal gravimetric experiments exhibited relatively high thermal stability of the F-Cu nanosheets with two decomposition temperatures at 273 °C (68.8%) and 332 °C (14.3%) (Supplementary Fig S2).

Evaluation of the catalytic performance of F-Cu bionanozymes

2D layered nanomaterials have long been shown to be excellent materials of choice in the field of catalysis due to their unique structural and electronic properties originating from their ultrathin morphology and large surface area[37]. Therefore, the F-Cu crystals not only possess the advantages of easier and more rapid synthesis compared to natural enzymes, but also meet the prerequisites for an efficient catalytic system, an ultra-thin nanolayered structure accompanied by ample catalytically active redox sites, making them promising bionanozymes. Hence, the intrinsic catalytic activity of F-Cu nanosheets as mimicking laccase function was first evaluated by performing the benchmarked oxidation reaction of 2,4-dichlorophenol (2,4-DP) together with 4-aminoantipyrine (4-AP)[38]. Here, 2,4-DP is the real substrate, and the radical product of its F-Cu bionanozyme- or laccase- catalyzed oxidation reacts with 4-AP to generate a red-colored antipyrilquinoneimine dye with characteristic broad absorbance centered at 510 nm (Fig. 3a and 3b). The 2,4-DP and 4-AP reaction mixture in the absence of a catalyst did not show any significant coloration and product absorption peak. F-Cu nanosheets generated a more intensely colored product and corresponding 510 nm absorption band compared to laccase (Fig 3b, Supplementary Movie S4) at the same weight percent (0.1 mg/mL), suggesting that F-Cu possesses an outstanding laccase-mimicking catalytic activity. Further, the dependence of the initial rate of the reaction on substrate concentration for F-Cu was consistent with its enhanced activity compared to the laccase enzyme (Fig. 3c). The typical Michaelis–Menten model fitting corroborated the enzyme-like catalytic characteristics of F–Cu nanosheets, with maximum initial velocity (V_{max}) = 6 ´ 10^{-5} mMs^{-1}, Michaelis–Menten constant (K_m) = 0.19 mM and catalytic efficiency (k_{cat}/K_m) = 0.2 $M^{-1}s^{-1}$, while laccase displayed V_{max}= 3 ´ 10^{-6} mMs^{-1}, K_m = 0.06 mM and k_{cat}/K_m= 0.02 $M^{-1}s^{-1}$. Moreover, F-Cu utilizes a single amino acid (F), making this system much less complex than the laccase enzyme comprising a primary sequence of several hundred amino acid. Hence, in terms of molecular mass, F-Cu is the smallest known laccase mimicking bionanozyme and exhibits three orders ($k_{cat}/K_M = 5 ´ 10^{-4} (g\,l^{-1})^{-1}\,s^{-1}$) of greater catalytic efficiency than the native laccase enzyme ($k_{cat}/K_M = 2.5 ´ 10^{-7} (g\,l^{-1})^{-1}\,s^{-1}$) (Table 1). To further confirm the role of the F-Cu bionanozyme, control experiments were carried out using all possible combinations of catalyst building blocks. As shown in Fig. 3d, apart from F-Cu, all other combinations did not show any significant catalytic activity, except for Cu^{2+} alone which produced a light color product with only 16% activity relative to F-Cu. These results indicate that the catalytic activity indeed depends on the F-Cu nanosheets rather than any non-assembled free F and Cu^{2+} ionic species. To better understand the chemical catalysis mechanism, copper complexes of three different amino acids (basic amino acid glycine (G-Cu) and the amino acids present at the laccase active center: histidine (H-Cu) and cysteine (C-Cu)) were synthesized, and their catalytic activities were compared to that of the F-Cu bionanozyme (Fig. 3e). Among these, the F-Cu nanozyme displayed the highest activity (100%), followed by G-Cu (25%), H-Cu (19%), Cu^{2+} ions

(16%) and C-Cu (1.5%). Next, we replaced the divalent copper ions with zinc ions (Zn^{2+}) by preparing an F-Zn complex and tested its catalytic activity. However, F-Zn showed a negligible activity (1.4%, Fig. 3e), emphasizing the crucial role of Cu^{2+} in this reaction, similar to natural laccases. Therefore, the interaction between Cu^{2+} and F to form a highly crystalline 2D layered nanostructure is required for the catalytic activity, while the carboxylate and amine functional groups in the amino acid skeleton support the coordination sites without contributing much to catalysis.

Table 1. Kinetic parameters of F-Cu bionanozyme and laccase enzyme for oxidizing 2,4-DP at 25 °C.

Catalyst	#AA	M.Wt (Da)	k_{cat}/K_m ($M^{-1}s^{-1}$) ´10^{-1}	k_{cat}/K_m (($g\ l^{-1}$)$^{-1}$ s^{-1}) ´10^{-5}
F-Cu	1	392	2	50
Laccase	~ 521	~ 80,000	0.2	0.02

#AA = number of amino acids, M.Wt = molecular weight.

Many oxidases, such as glucose oxidase, accelerate a similar phenol oxidation reaction via catalytic reduction of O_2 to H_2O_2. In contrast, laccase directly reduces molecular oxygen to water without any production or requirement of H_2O_2. To test whether H_2O_2 was generated during the reaction catalyzed by the F-Cu bionanozyme, a reaction mixture of 2,4-DP and F-Cu (4-AP was omitted to avoid interference of red color) was centrifuged (Fig. 3f). 2,2'-azino-bis(3-ethylbenzothiazoline-6-sulfonic acid (ABTS) and horseradish peroxidase (HRP) were added to the supernatant, yet no variation of color or absorption was observed (inset of Fig. 3f), indicating the absence of H_2O_2. However, under similar conditions, the addition of H_2O_2 resulted in a green color solution with intense absorbance at 415 nm, characteristic of ABTS oxidized product. These results further confirm that the F-Cu bionanozyme is indeed a laccase mimic rather than any other oxidase that generates an H_2O_2 byproduct. Since the laccase activity depends on molecular oxygen, we further tested the oxygen dependency of the F-Cu catalytic activity by conducting the reaction in the presence (open to air) and absence (nitrogen gas bubbled solution) of an oxygen-containing environment (Supplementary Fig S5). Interestingly, the catalytic reaction rate in the presence of atmospheric oxygen was 2.5-fold higher than in the absence of oxygen. This confirms the oxygen dependency of F-Cu catalyzed oxidation of phenols, similar to the natural laccase enzyme. The oxidation state of Cu^{2+}within the F-Cu bionanozyme during the reaction was probed through electron paramagnetic resonance (EPR) spectroscopy (Supplementary Fig S5). The F-Cu bionanozyme alone displayed an intense EPR signal at 3291 G characteristic of Cu^{2+}. However, the addition of 2,4-DP to the F-Cu reaction mixture resulted in diminished EPR signal, suggesting that the reduction of Cu^{2+} to Cu^{1+} took place, in line with the anticipated laccase mimicking redox catalytic mechanism. To visualize the progress of the F-Cu bionanozyme catalytic oxidation of 2,4-DP, *in-situ* microscopy (Supplementary Movie S3) experiments were performed for 1 h at 15-sec intervals (Fig. 3g). The colorless reaction mixture turned into a strong

red color on the surface of the 2D F-Cu crystals without affecting their morphology, providing further evidence of the catalytic function of the F-Cu 2D crystals.

Catalytic stability, recyclability and substrate universality of F-Cu bionanozymes

To demonstrate its practical utility, we investigated the relative stability of the F-Cu bionanozyme compared to laccase in various extreme experimental conditions including pH, ionic strength, storage time and temperature. Specifically, the catalytic assay was performed in PBS buffer (1X, 25 °C) at different pH values ranging from pH 3.0 to 9.0. As shown in Fig. 4a, laccase lost its catalytic activity after incubation in a strongly acidic pH 3.0 (5%) and basic pH 9.0 (48%), while the F-Cu bionanozyme maintained at least 60% of its catalytic activity at pH 3.0 and gradually increased at pH 4.0-9.0 (65%–120%). The influence of ionic strength on catalytic activity was tested at different NaCl concentrations ([NaCl] = 0 to 600 mM). The increase of ionic strength induced a drastic decrease in laccase activity (from 100% to 1.4%) due to the salting-out effect and chloride ion inactivation (Fig. 4b). In contrast, F-Cu showed a gradually increasing activity (100% to 360%) with elevated NaCl concentration. This result prompted us to test the catalysis in actual water samples including tap water, river water, and seawater (Supplementary Fig S4). F-Cu and laccase showed similar relative activity in both tap and river water. However, in seawater, laccase completely lost its activity, while F-Cu retains 76% of its catalytic activity. Therefore, the F-Cu bionanozyme is robust enough for on-field phenol oxidation in water samples highly relevant for public health. Next, the storage stability was estimated by loading the catalyst in PBS buffer (1X, pH 7.4) at 25 °C and assayed every 5 days for one month. As shown in Fig. 4c, laccase relative activity was gradually decreased over storage time and became completely inactive on the 10^{th} day. However, the F-Cu bionanozyme retained almost 90% of activity after 30 days of storage, as well as remained 95% active after 210 days of storage in air at room temperature, indicating the excellent stability of the F-Cu bionanozyme during storage either in water or in air. Further, thermal stability was evaluated by incubating F-Cu and laccase at different temperatures ranging from 273 K to 373 K for 1 hour followed by a catalytic activity assay at room temperature (Fig. 4d). Due to thermal denaturation, the relative activity of laccase decreased gradually and was completely lost at 330 K. On the other hand, F-Cu bionanozymes exhibited good thermal stability by retaining 92% activity even the following incubation at 373 K. To demonstrate the recyclability of the F-Cu bionanozymes, both 2,4-DP and 4-AP were mixed with F-Cu in PBS buffer (1X, at 25 °C) for each cycle. After each reaction cycle, the F-Cu bionanozyme was collected by centrifugation, washed with double distilled water and re-used for the next reaction cycle (Fig. 4e).

Remarkably, the F-Cu bionanozyme retained more than 80% of its relative activity even after fifteen cycles, while laccase is unable to be recycled. These results suggest that compared to natural laccase, the F-Cu bionanozyme shows higher catalytic stability and recyclability. To assess the substrate universality, F-Cu and laccase were mixed with various toxic phenolic contaminants and the catalytic oxidation activity was assayed (Fig. 4f). Interestingly, the F-Cu bionanozyme could not only catalyze the oxidation of all phenolic contaminants tested, but also showed higher catalytic activities compared to laccase, demonstrating the favorable substrate universality of the F-Cu bionanozyme. Importantly, F-Cu

showed a higher conversion rate of chlorophenols (2,4-DP and 2,4,6-trichlorophenol) which are listed by the U. S. Environmental Protection Agency (EPA) as priority environmental pollutants [39].

Reaction pathway for F–Cu catalytic oxidative coupling of phenolic pollutants

To understand the energetics of phenoxyl radical formation, we carried out first-principle spin-polarized density functional theory calculations on a cluster model of F-Cu comprised of four $Cu(F)_2$ units as shown in Fig. 5a (left). Our cluster model resembles an edge of the F-Cu crystal (100) surface. To obtain the energetics of the entire reaction, we added one oxygen, two water, and two phenol molecules to this tetramer model of F-Cu. Furthermore, to mimic periodic crystal effects, we fixed the positions of two of the four $Cu(F)_2$ units (located on the right side of the tetramer, represented with both sticks and transparent beads).

The entire reaction starts with a phenol molecule approaching the active copper site (step 1). In this step, the spin-density is primarily located near the four copper sites (see S1 in Fig. 5b) and on the oxygen molecule. Next, there is a transfer of a hydrogen atom from the phenol molecule to one of the COO groups of the F moiety (step 2), with an energy barrier of ~ 29 kcal/mol. Step 2 is ~ 22 kcal/mol higher in energy than step 1, and due to the transfer of a hydrogen atom from the phenol, a phenoxyl radical is formed in this step. We confirmed the formation of a phenoxyl radical through spin-density plots (Fig. 5b), where we observed an accumulation of spin-density on the phenyl moiety of the phenol in step 2, which was absent in step 1. In the next step, the hydrogen atom is further transferred from the COO group to the oxygen molecule, with an energy barrier of ~ 9.5 kcal/mol. In the experimental studies, molecular oxygen is readily available in the solvent (water) as dissolved oxygen. Until step 3, the reaction is energetically uphill; however, once this phenoxyl radical diffuses from the active copper site, it interacts with other phenoxyl radicals forming the respective polymers, resulting in an overall exothermic reaction. To simulate this downhill process, we studied the formation of a dimer (2,2'-biphenol) from two phenols. To reduce the computational burden associated with the simulation of this large system, we assumed that both phenols interact with the adjacent copper sites.

In step 4, we observed the formation of two phenoxyl radicals on the adjacent copper sites, where the oxygen molecule receives the protons from both phenols. The spin-density plots confirm the radical nature of the phenoxyl moieties. It is interesting to note that this configuration containing two phenoxyl radicals on adjacent copper sites is only slightly higher in energy (~ 2 kcal/mol) compared to step 3. Finally, the two radicals combine with each other to form the polymerized product that is ~ 55 kcal/mol lower in energy compared to step 3 or step 4.

Detection of catecholamine neurotransmitter using the F-Cu bionanozyme

To further broaden the scope of the F-Cu bionanozyme, we examined the catalytic oxidation of catecholamines, biologically important phenolic neurotransmitters (dopamine (DA), epinephrine (EP), norepinephrine (NE) and L-DOPA (LD)). Catecholamines play a vital role in various functions of the cardiovascular, nervous, and endocrine systems[40]. Therefore, any disruption in their concentration levels

may induce diverse diseases including Parkinson's disease, schizophrenia, and even tumors such as paraganglioma and pheochromocytoma. On the other hand, catecholamines are extensively used as drugs for emergency heart disease, anaphylactic shock, and bronchial asthma. Hence, the detection and quantitative analysis of catecholamines are essential for disease diagnosis and pharmaceutical assessments. Interestingly, simple mixing of F-Cu or laccase with EP resulted in gradual color change in the solution from colorless to intense red, indicating the formation of an oxidized product (Fig. 6a). This was further evident from the appearance of a new absorption band centered at 485 nm, characteristic of an adrenochrome product (Fig. 6b). In contrast, in the absence of a catalyst (F-Cu or laccase), EP did not produce a significant color change. The F-Cu bionanozyme catalyzed product absorption, and solution coloration was much higher those observed for laccase. The catalytic course of F-Cu and laccase monitored at 485 nm over 30 min is shown in Fig. 6c. Remarkably, in the first 10 min, the reaction kinetics with the F-Cu bionanozyme is 20-fold faster than that of laccase. Furthermore, the calculated kinetics parameter V_{max} of the F-Cu bionanozyme is approximately ~43-fold higher than that of laccase. The catalytic colored oxidized product might be used as a method for the detection and quantification of EP. To test this option, we monitored the absorbance of the product at 485 nm as a function of EP concentration in the presence of the same mass concentration (0.1 mg/mL) of the F-Cu bionanozyme and laccase (Fig. 6d and 6e). Both F-Cu and laccase displayed a linear relationship between the product absorbance and the concentration of EP between 20 mM to 100 mM. The obtained limit of detection (LOD) of EP is 150 nM in the presence of the F-Cu bionanozyme, compared to 5 mM in the presence of laccase. Accordingly, F-Cu is approximately 36-fold more sensitive than laccase. Therefore, the method utilizing the F-Cu bionanozyme is much more simple, ultrasensitive, and allows the same conversion rate *via* an approximately ~5400 fold more cost-effective reaction compared to the natural enzyme laccase. Next, we analyzed the catalytic oxidation of other catecholamines (DA, NE and LD) in the presence of the F-Cu bionanozyme and laccase. As shown in Fig. 6f, the F-Cu bionanozyme could catalyze the oxidation of all types of catecholamine molecules more effectively than laccase. Therefore, based on the F-Cu bionanozyme catalytic oxidation reactions, a rapid, economical, and ultrasensitive methodology has been developed for the colorimetric determination of catecholamine neurotransmitters.

Conclusions

In conclusion, we describe an important step towards the goal of developing eco-friendly, cost-effective, efficient, stable, and reusable minimalist bionanozymes for environmental remediation. Unlike natural enzymes consisting of several hundred amino acid sequences, the designed F-Cu bionanozyme utilizes only a single amino acid, F, which spontaneously coordinates with Cu^{2+} ions to produce catalytically ideal hierarchical 2D layered van der Waals crystals. This simple supramolecular approach provides an attractive new alternative to the expensive, time-consuming, and inaccessible chemical synthesis and purification processes. The F-Cu bionanozyme reported here uses 2D orderly spaced Cu^{2+}/Cu^{1+} sites for mimicking the biocatalytic action of the natural enzyme laccase and effectively oxidizes a broad range of widespread environmentally toxic phenolic contaminants and serves as an ultrasensitive tool to detect biologically important neurotransmitters. The ultrathin 2D layered structure of the F-Cu bionanozyme

provides a high surface area and a larger number of active sites accessibility, thus showing a catalytic property per weight 10-fold higher than the laccase enzyme. Compared to the natural laccase enzyme, the developed F-Cu bionanozyme displays excellent stability under extreme conditions, recyclability, and wide substrate universality, thus bearing great potential for environmental remediation, industrial and healthcare applications. The ease with which we were able to develop the robust single amino acid bionanozyme might provide an important missing link in the quest for the prebiotic catalysts during the evolution of enzymes. Moreover, given the rich structural diversity and versatile metal coordination characteristics of amino acids, this report provides a rational path towards the *de novo* design of next-generation minimalistic bionanozymes for energy, environment, and healthcare applications.

Materials And Methods

Materials

L-phenylalanine (F), Glycine (G), L-Cysteine (C), L-Histidine (H) Copper (II) chloride dihydrate ($CuCl_2$), Sodium hydroxide (NaOH), 2,4-dichlorophenol (2,4-DP), 4-aminoantipyrine (4-AP), 2,2'-azino-bis(3-ethylbenzothiazoline-6-sulfonic acid (ABTS), Peroxidase from horseradish (HRP), Hydrogen peroxide solution (H_2O_2), N-Methyl-2-pyrrolidone (NMP), phenol, Catechol, Hydroquinone, 2-Aminophenol, 2,6-Dimethoxyphenol, 2-Naphthol, 2-Nitrophenol, 2,4,6-trichlorophenol, epinephrine (EP), norepinephrine (NP), dopamine, L-DOPA, Sodium chloride (NaCl), Potassium chloride (KCl), Disodium phosphate (Na_2HPO_4), and Potassium phosphate monobasic (KH_2PO_4) were purchased from Sigma-Aldrich (Rehovot, Israel). All materials were used as received. Milli-Q water was used to prepare all the buffers and solutions.

Preparation of F-Cu single crystals

One equivalent of the $CuCl_2$ (5 mM) aqueous solution was slowly added to two equivalents of L-phenylalanine (10 mM) alkaline solution (containing NaOH (10 mM)) under heating (60 °C). Thin plate-like crystals were spontaneously formed at the liquid-air interface. The crystals were collected by filtration and washed with an excess of double-distilled water and ethanol. The *in-situ* crystal growth was recorded using optical microscopy at 14-second intervals.

Single crystal X-ray data collection and processing

Blue plate-like crystals suitable for diffraction were coated with Paratone oil (Hampton Research) and mounted on MiTeGen loops and flash frozen in liquid nitrogen. All X-ray diffraction measurements were done at 100K. Diffraction measurements for F-Cu crystals were done at the ESRF synchrotron, station ID23-1. Data were collected and processed using MXCube and the automated XDS pipeline. The structure was solved by direct methods using SHELXT-2013 or SHELXT 2016/4. The structure was refined by full-matrix least-squares against F2 with SHELXL 2016/4. The crystallographic data are given in Table S1. The structure was illustrated using Mercury 3.9 (Cambridge Crystallographic Data Centre, Cambridge, UK).[1]

Powder X-ray diffraction

The F-Cu nanosheets were deposited on a quartz zero-background sample holder, and powder XRD was performed on Bruker D8 Advance X-ray powder diffractometer (Bruker) at room temperature between 5 and 45° 2θ. The background was subtracted to exalt the diffraction peaks.

FTIR spectroscopy

The F-Cu nanosheets were deposited on disposable KBr infrared sample cards (Sigma-Aldrich), and subsequently allowed to dry under vacuum. The spectra were collected from 4000 to 400 cm^{-1} at room temperature using a nitrogen-purged Nicolet Nexus 470 FTIR spectrometer (Nicolet) equipped with a deuterated triglycine sulfate detector. One hundred and twenty-eight scans were collected with a spectral resolution of 4 cm^{-1}. The background was subtracted from a control KBr spectrum.

High-resolution scanning electron microscopy (HRSEM)

The as-prepared F-Cu crystals were deposited on a clean microscope glass coverslip and coated with Cr. The images were recorded under aJSM-6700 field emission scanning electron microscope (JEOL, Tokyo, Japan) operated at 10 kV.

Atomic force microscopy (AFM)

The F-Cu crystals before and after ultrasonication treatment (for 10 min) were deposited onto a clean microscope glass coverslip. The samples were characterized using the AIST-NT Smart AFM system in non-contact (tapping) mode, 100-mm-long silicon nitride cantilevers (OMCL-RC800PSA-W, Olympus) with a resonance frequency of 70 kHz. The images were analyzed and visualized using WSxM imaging software (Nanotec Electronica S.L).

Thermal gravimetric analysis (TGA)

TGA experiments were performed on a TA Instruments (USA) module SDT 2950, at a temperature range between 40 °C and 510 °C, with a heating rate of 10 °C min^{-1}, under dry ultrahigh-purity argon atmosphere.

Catalytic assay and kinetic parameters determination

The F-Cu bionanozyme catalytic performance was measured by the chromogenic reaction of phenolic compounds with 4-AP using a 96-well UV-Star UV transparent flat bottom plate (Greiner BioOne, Frickenhausen, Germany). First, 4-AP (30 µL from 1 mg/mL aq. solution,) and 2,4-DP (30 µL from 1 mg/mL aq. solution) solutions were mixed with PBS buffer (1X, pH 7.4, 210 µL). Next, F-Cu bionanozyme in NMP or laccase enzyme (30 µL from 1 mg/mL) was added. The reaction progress was monitored at 510 nm using a Biotek Synergy HT plate reader (Biotek, Winooski, VT, USA) at 22 °C and continuous stirring mode. To obtain the initial reaction rate (V0) various concentrations of 2,4-DP (0.02, 0.04, 0.06,

0.08, 0.1, 0.2, 0.3 0.4, 0.5, 0.6 and 0.7 mM) were respectively reacted with 0.1 mg/mL of 4-AP, catalyzed by 0.1 mg/mL of F-Cu bionanozyme or laccase. The average of the V_0 values was plotted as a function of substrate concentration and fit to the Michaelis–Menten equation ($V_0 = V_{max}[S] / (K_M + [S])$ to obtain the kinetic parameters V_{max} and K_M. The k_{cat}/K_M values were obtained by fitting the linear portion of the Michaelis–Menten plot to $V_0 = (k_{cat}/K_M)[E][S]$. All measurements were replicated at least three times and averaged for accuracy. The other phenolic substrates (phenol, Catechol, Hydroquinone, 2-Aminophenol, 2,6-Dimethoxyphenol, 2-Naphthol, 2-Nitrophenol, and 2,4,6-trichlorophenol) at 0.1 mg/mL were reacted with 0.1 mg/mL 4-AP in PBS buffer (1X, pH 7.4, 210 µL) containing 0.1 mg/mL of F-Cu bionanozyme. The *in-situ* experiments were done under an optical microscope by mixing 0.1 mg/mL of 2,4-DP and 4-AP with F-Cu crystals (0.1 mg/ml) PBS buffer (1X, pH 7.4, 210 µL) solution. The reaction progress was recorded at 15-sec intervals.

Assessment of catalytic stability comparison

To know the effect of pH, F-Cu bionanozyme or laccase catalytic assay was performed in a similar way but at different pH (3.0–9.0) PBS buffer (1X) solutions. The relative activity is compared with that of pH 7. Different concentrations of NaCl (0, 50, 100, 200, 400, 500, and 600 mM) were added into the reaction mixture to measure the effect of ionic strength on the catalytic activity, and the relative activity was compared with that of 0 mM NaCl. To assess the practical utility of our enzymes, the F-Cu bionanozyme, and laccase catalytic assays were measured in real water (instead of PBS buffer) including tap water, river water, and seawater as described above. The long-term storage stability was measured every 5 days for the residual activity of F-Cu bionanozyme or laccase enzyme dispersed in Milli-Q water stored at room temperature. The activity on the 0^{th} day was taken as a reference. The effect of temperature was measured by incubating the F-Cu bionanozyme and laccase enzyme separately at 0, 20, 40, 60, 80, and 100 °C for 30 min, and their catalytic activity was subsequently assayed. The activity at 0 °C was taken as a reference. To evaluate the recyclability of F-Cu bionanozyme, the solutions of 2,4-DP (0.1 mg/mL), 4-AP (0.1 mg/mL), and F-Cu (0.1 mg/mL) were mixed in PBS buffer (1X, pH=7.4,) at 25 °C, and the reaction was assayed for 1 h per cycle. After each reaction cycle the F-Cu, the bionanozyme was collected by centrifugation (12,000 rpm, 3 min), washed with Milli-Q water 3 times, and re-used for the next reaction cycle.

Reaction with Epinephrine

The F-Cu bionanozyme or laccase enzyme (30 µL from 1 mg/mL solution) and epinephrine (30 µL from 1 mg/mL aq. solution,) were mixed with PBS buffer (1X, pH 7.4, 240 µL) in a 96-well UV-Star UV transparent flat bottom plate (Greiner BioOne, Frickenhausen, Germany). The reaction progress was monitored at 485 nm using a Biotek Synergy HT plate reader (Biotek, Winooski, VT, USA) at 22 °C and continuous stirring mode. To evaluate the detection limit of epinephrine, different concentrations of epinephrine (0, 20, 40, 60, 80, and 100 µM) were mixed with 0.1 mg/mL of F-Cu bionanozyme or laccase in the PBS buffer for 1 h at 25 °C before the 485 nm absorbance measurement. The limit of detection was calculated by 3σ/b, where σ is the standard deviation of the blank signals, and b is the slope of the regression line.

Computational Details

Spin-polarized density functional theory (DFT) calculations were performed using the PBE[1] exchange-correlation functional and the numerical orbital basis-sets as implemented in the all-electron code FHI-aims.[2] Dispersion interactions were included using the Tkatchenko and Scheffler scheme.[3] For each geometry, different spin-configurations were considered, and the configuration with the lowest energy was reported (a heptet configuration was used for steps 1 through 4 and a quintet was used for step 5. For step 3, the triplet and heptet configurations were found to be degenerate). In all calculations, we used a convergence criterion of 10^{-5} for the electron density and 10^{-2} eV $Å^{-1}$ for the structural relaxation. Throughout these calculations, we used the "tight" settings for all the atomic species as available in the FHI-aims software package (the difference in the energies predicted using the "light" and "tight" settings were found to be less than 1 kcal/mol). For the climbing image calculations,[4,5] we used "Climb_mode=2", which corresponds to the optimization of both the climbing image as well as the two images close to it, and a convergence criterion of 0.05 eV $Å^{-1}$ was utilized while evaluating the forces.

Declarations

Acknowledgments

This work was partially supported by a grant from the European Research Council under the European Union's Horizon 2020 research and innovation program (BISON, Advanced ERC grant, no. 694426) (to E.G.). P.M. gratefully acknowledges the Center for Nanoscience and Nanotechnology of Tel Aviv University for a postdoctoral fellowship, S.S.R.K.C.Y. and B.M.W. acknowledges the support of the National Science Foundation under Grant No. CBET-1833218 and the Extreme Science and Engineering Discovery Environment (XSEDE) Comet computing cluster at the University of California, San Diego, through allocation TG-ENG160024. We also thank S. Rencus-Lazar for linguistic editing and the members of the Gazit laboratory for helpful discussions.

Author contributions

P.M. and E.G. conceived and designed the experiments. P.M. grew the single crystals of the catalytic complex and performed all the experiments and analyzed the data. L.J.W.S. collected the single-crystal diffraction data and solved the crystal structure. S.S.R.K.C.Y. and B.M.W. performed the computational studies. P.M. and E.G. wrote and edited the manuscript. All authors discussed and commented on the manuscript.

Competing Financial Interests

The authors declare no competing interests.

Corresponding author

Correspondence to Ehud Gazit (ehudg@post.tau.ac.il) and Bryan M. Wong (bmwong@engr.ucr.edu)

Additional information

Supplementary information and Supplementary movies are available for this paper

Competing interests

Authors declare no competing interests

Data Availability Statement

The X-ray crystallographic coordinates for the structure reported in this study have been deposited at the Cambridge Crystallographic Data Centre (CCDC), under deposition 1871975.

References

1. Benkovic, S. J. A perspective on enzyme catalysis. *Science* **301**, 1196–1202 (2003).
2. DeGrado, W., Wasserman, Z. & Lear, J. Protein design, a minimalist approach. *Science* **243**, 622–628 (1989).
3. Miller, S. L. & Urey, H. C. Organic compound synthesis on the primitive earth. *Science* **130**, 245–251 (1959).
4. Carny, O. & Gazit, E. A model for the role of short self-assembled peptides in the very early stages of the origin of life. *FASEB J.* **19**, 1051–1055 (2005).
5. Vendruscolo, M. & Dobson, C. M. Dynamic visions of enzymatic reactions. *Science* **313**, 1586–1587 (2006).
6. Koeller, K. M. & Wong, C.-H. Enzymes for chemical synthesis. *Nature* **409**, 232–240 (2001).
7. Aldridge, S. Industry backs biocatalysis for greener manufacturing. *Nat. Biotechnol.* **31**, 95–96 (2013).
8. Schmid, A. *et al.* Industrial biocatalysis today and tomorrow. *Nature* **409**, 258–268 (2001).
9. Rao, M. A., Scelza, R., Acevedo, F., Diez, M. C. & Gianfreda, L. Enzymes as useful tools for environmental purposes. *Chemosphere* **107**, 145–162 (2014).
10. Torres, E., Bustos-Jaimes, I. & Le Borgne, S. Potential use of oxidative enzymes for the detoxification of organic pollutants. *Appl. Catal. B Environ.* **46**, 1–15 (2003).
11. Mate, D. M. & Alcalde, M. Laccase: a multi-purpose biocatalyst at the forefront of biotechnology. *Microb. Biotechnol.* **10**, 1457–1467 (2017).
12. Rodríguez-Delgado, M. M. *et al.* Laccase-based biosensors for detection of phenolic compounds. *TrAC Trends Anal. Chem.* **74**, 21–45 (2015).
13. Gao, L. *et al.* Intrinsic peroxidase-like activity of ferromagnetic nanoparticles. *Nat. Nanotechnol.* **2**, 577–583 (2007).

14. Jiang, D. *et al.* Nanozyme: new horizons for responsive biomedical applications. *Chem. Soc. Rev.* **48**, 3683–3704 (2019).
15. Wu, J. *et al.* Nanomaterials with enzyme-like characteristics (nanozymes): next-generation artificial enzymes (II). *Chem. Soc. Rev.* **48**, 1004–1076 (2019).
16. Huang, Y., Ren, J. & Qu, X. Nanozymes: classification, catalytic mechanisms, activity regulation, and applications. *Chem. Rev.* **119**, 4357–4412 (2019).
17. Wang, X., Liu, J., Qu, R., Wang, Z. & Huang, Q. The laccase-like reactivity of manganese oxide nanomaterials for pollutant conversion: rate analysis and cyclic voltammetry. *Sci. Rep.* **7**, 7756 (2017).
18. Gupta, S. S. Rapid total destruction of chlorophenols by activated hydrogen peroxide. *Science* **296**, 326–328 (2002).
19. Makam, P. & Gazit, E. Minimalistic peptide supramolecular co-assembly: expanding the conformational space for nanotechnology. *Chem. Soc. Rev.* **47**, 3406–3420 (2018).
20. Tao, K., Makam, P., Aizen, R. & Gazit, E. Self-assembling peptide semiconductors. *Science* **358**, eaam9756 (2017).
21. Zhang, S. Fabrication of novel biomaterials through molecular self-assembly. *Nat. Biotechnol.* **21**, 1171–1178 (2003).
22. Marshall, L. R., Zozulia, O., Lengyel-Zhand, Z. & Korendovych, I. V. Minimalist de novo design of protein catalysts. *ACS Catal.* **9**, 9265–9275 (2019).
23. Zozulia, O., Dolan, M. A. & Korendovych, I. V. Catalytic peptide assemblies. *Chem. Soc. Rev.* **47**, 3621–3639 (2018).
24. Omosun, T. O. *et al.* Catalytic diversity in self-propagating peptide assemblies. *Nat. Chem.* **9**, 805–809 (2017).
25. Singh, N., Kumar, M., Miravet, J. F., Ulijn, R. V. & Escuder, B. Peptide-based molecular hydrogels as supramolecular protein mimics. *Chem. Eur. J.* **23**, 981–993 (2017).
26. Guler, M. O. & Stupp, S. I. A self-assembled nanofiber catalyst for ester hydrolysis. *J. Am. Chem. Soc.* **129**, 12082–12083 (2007).
27. Dear, A. J. *et al.* The catalytic nature of protein aggregation. *J. Chem. Phys.* **152**, 045101 (2020).
28. Lengyel, Z., Rufo, C. M., Moroz, Y. S., Makhlynets, O. V. & Korendovych, I. V. Copper-containing catalytic amyloids promote phosphoester hydrolysis and tandem reactions. *ACS Catal.* **8**, 59–62 (2018).
29. Bolisetty, S. & Mezzenga, R. Amyloid–carbon hybrid membranes for universal water purification. *Nat. Nanotechnol.* **11**, 365–371 (2016).
30. Singh, N., Tena-Solsona, M., Miravet, J. F. & Escuder, B. Towards supramolecular catalysis with small self-assembled peptides. *Isr. J. Chem.* **55**, 711–723 (2015).
31. Faiella, M. *et al.* An artificial di-iron oxo-protein with phenol oxidase activity. *Nat. Chem. Biol.* **5**, 882–884 (2009).

32. Makam, P. *et al.* Non-proteinaceous hydrolase comprised of a phenylalanine metallo-supramolecular amyloid-like structure. *Nat. Catal.* **2**, 977–985 (2019).
33. Liang, H. *et al.* Multicopper laccase mimicking nanozymes with nucleotides as ligands. *ACS Appl. Mater. Interfaces* **9**, 1352–1360 (2017).
34. Ren, X., Liu, J., Ren, J., Tang, F. & Meng, X. One-pot synthesis of active copper-containing carbon dots with laccase-like activities. *Nanoscale* **7**, 19641–19646 (2015).
35. Adler-Abramovich, L. *et al.* Phenylalanine assembly into toxic fibrils suggests amyloid etiology in phenylketonuria. *Nat. Chem. Biol.* **8**, 701–706 (2012).
36. Shaham-Niv, S., Adler-Abramovich, L., Schnaider, L. & Gazit, E. Extension of the generic amyloid hypothesis to nonproteinaceous metabolite assemblies. *Sci. Adv.* **1**, e1500137 (2015).
37. Deng, D. *et al.* Catalysis with two-dimensional materials and their heterostructures. *Nat. Nanotechnol.* **11**, 218–230 (2016).
38. Ge, J., Lei, J. & Zare, R. N. Protein–inorganic hybrid nanoflowers. *Nat. Nanotechnol.* **7**, 428–432 (2012).
39. Ramamoorthy, S. & Ramamoorthy, S. Chlorinated organic compounds in the environment (CRC Press, Boca Raton, FL, 1997).
40. Kagedal, B. & Goldstein, D. S. Catecholamines and their metabolites. *J. Chromatogr. B Biomed. Sci. Appl.* **429**, 177–233 (1988).

Figures

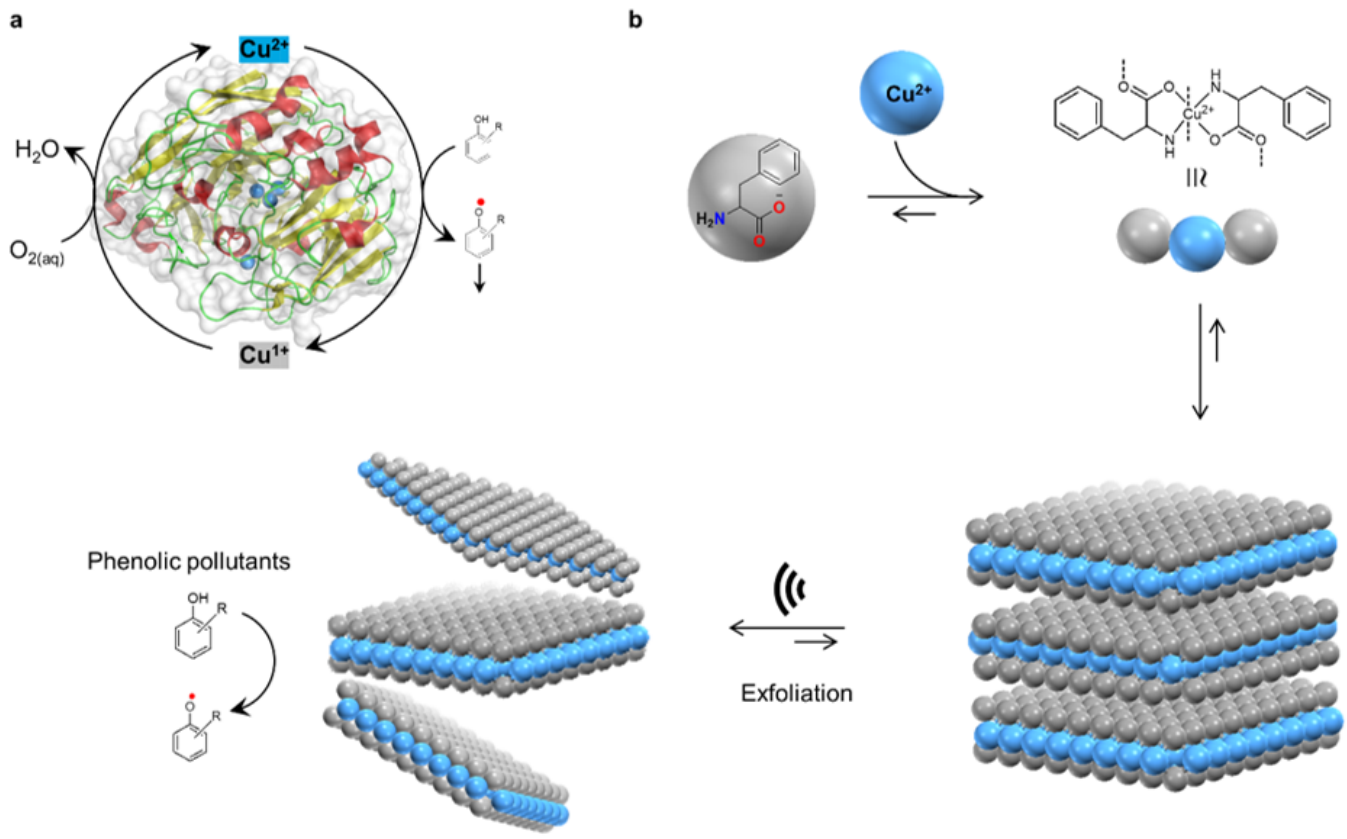

Figure 1

Bioinspired design of a laccase-mimicking F-Cu 2D layered bionanozyme. a, Structure of natural Laccase (PDB entry 1V10), which comprises a redox (Cu2+/Cu1+) multicopper-coordinated catalytic site involved in the catalytic oxidation of toxic phenolic compounds into phenoxy radicals via reduction of oxygen to water. b, Chemical structure and anticipated schematic illustration of F-Cu nanozyme formation. F spontaneously coordinates with Cu2+ via carboxylate, amine chelating modes into a hierarchical 2D van der Waals layered F-Cu structure. Further mechanical (ultrasonication) exfoliation to F-Cu monolayers facilitates laccase-mimicking oxidation of environmentally toxic phenol.

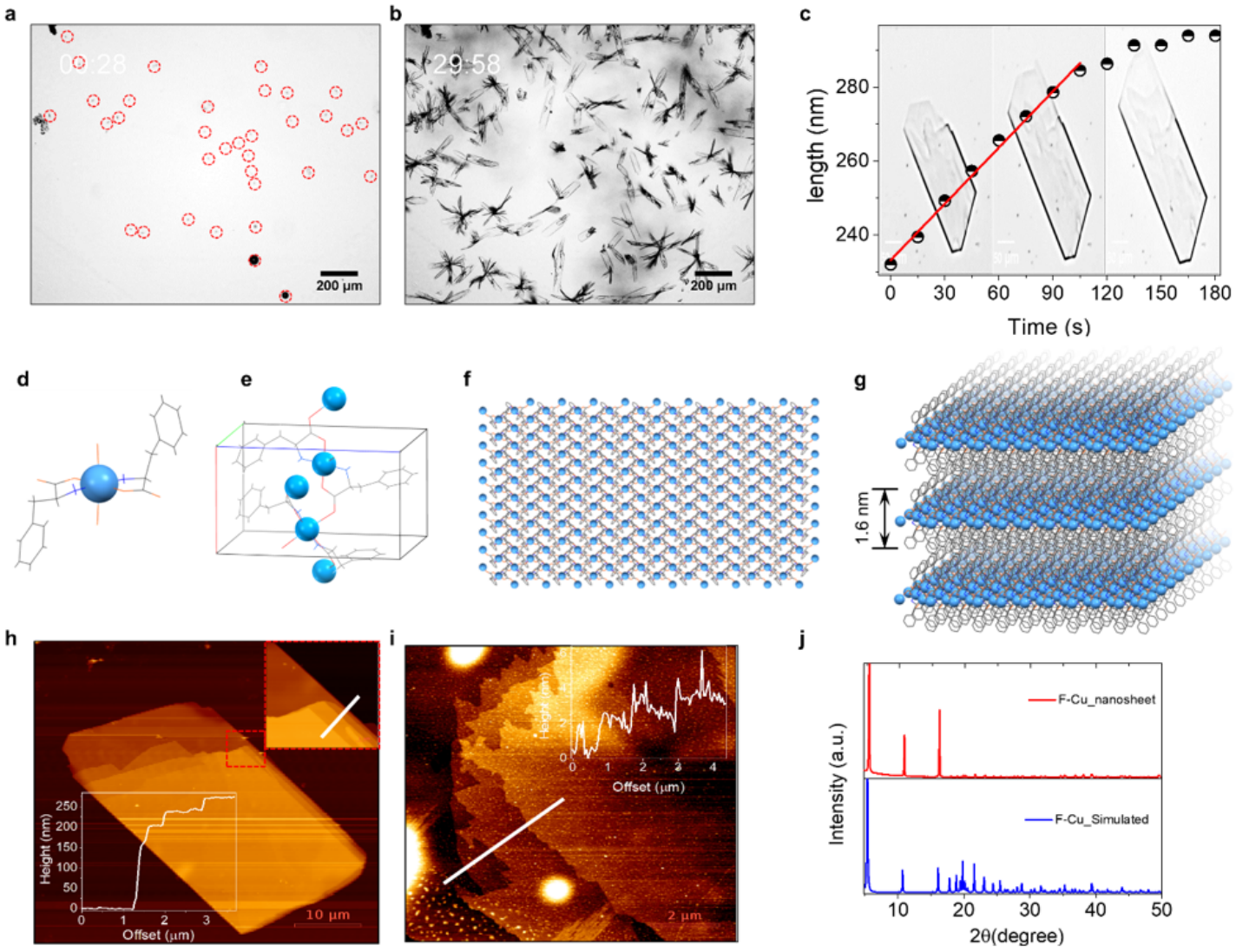

Figure 2

Structural characterization of F–Cu. a-b, Optical microscopy snapshots taken from the in-situ monitoring of the F-Cu crystallization process (Supplementary Movie S1), showing the formation of (a) small nucleation seeds (red dotted circles) at 28 sec and (b) grown micrometer-long 2D crystals at ~30 min. c, Optical microscopy snapshots are taken from Supplementary Movie S2, which monitors the in-situ crystallization kinetics of the F–Cu 2D layered crystals and corresponding graphical representations of the elongation rate. The calculated average measured elongation rate is 7.89 nm s−1. d-g, Single-crystal X-ray structure of F-Cu (d), F-Cu assembly exhibits octahedral primary coordination complex structure (e), The unit cell comprises four F molecules and two Cu2+ ions (f), 2D infinite layered F-Cu coordination complex structure shown along the crystallographic plane. g, Hierarchical 2D van der Waals layered stacked structure shown along the crystallographic plane. h-i, AFM images and height profiles of F-Cu 2D layered crystals (h) before and (i) after ultrasonication treatment. displaying the mechanical exfoliation of pristine 2D hierarchical layered F-Cu crystals into single or several-layered nanosheets. The AFM height profiles of nanosheets (≈1.8 nm thick) are in good agreement with the single atomic layer thickness in the

crystal structure ((□1.6 nm thick, g). j, PXRD patterns of simulated from F-Cu crystal structure and experimental 2D nanosheets.

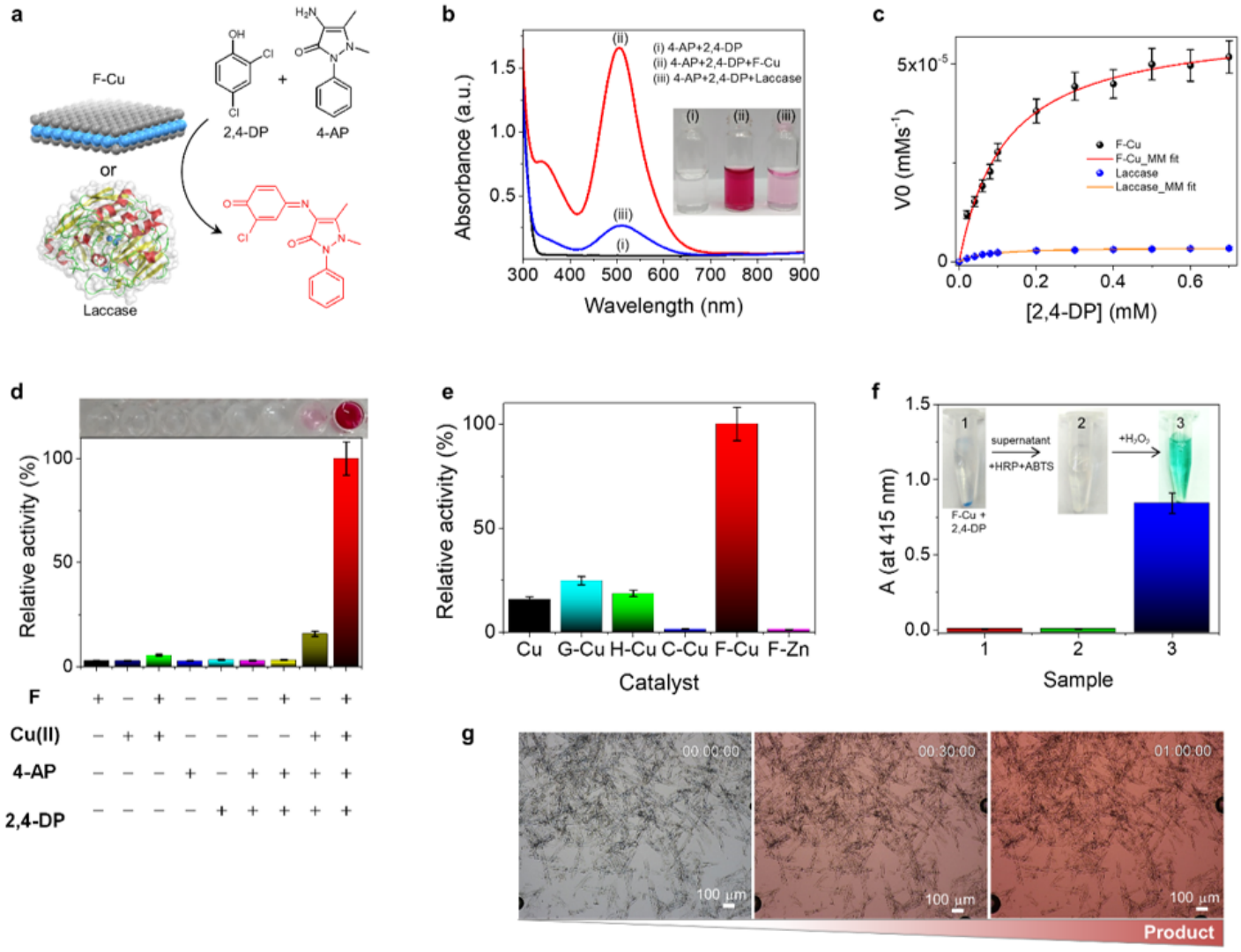

Figure 3

The laccase mimicking catalytic activity of F-Cu bionanozymes. a, Schematic illustration of the reaction utilizing 2,4-DP and 4-AP catalyzed by F-Cu nanosheets or laccase. b, UV–vis absorption spectra of (i) the two substrates and after reaction in the presence of (ii) F-Cu and (ii) laccase. Reaction conditions: 0.1 mg/mL 2,4-DP, 0.1 mg/mL 4-AP, 0.1 mg/mL F-Cu and 0.1 mg/mL Laccase in PBS buffer (1X), pH 7.25 at 25 □C. Inset: Photographs of the corresponding solutions. c, Initial rate (V0) of the reaction catalyzed by 0.1 mg/mL of F–Cu or laccase as a function of substrate concentration ([2,4-DP] = 0 – 0.5 mM, [4-AP] = 0.1 mg/mL). d, Relative catalytic activity in control experiments. No hydrolysis is observed when either F or Cu2+ is omitted from the system. e, Relative activity of several different amino acid-copper complexes. f, Control experiment testing the laccase mimicking activity of the F-Cu bionanozyme and the supernatant. Photographs of (1) F-Cu reacted with 2,4-DP in PBS buffer (1X) (pH 7.25 at 25 □C) after centrifugation, (2) the supernatant with ABTS and HRP added after centrifugation, and (3) after adding

H2O2 to (2). UV−vis absorbance at 415 nm of the corresponding samples is shown. g, Optical microscopy snapshots at different intervals (0 min, 30 min and 1 h) taken from the in-situ reaction monitoring of 2,4-DP and 4-AP catalyzed by F-Cu crystals (Supplementary Movie S3), displaying the solution color change going from colorless (at 0 min) to red (after 30 min and 1 h).

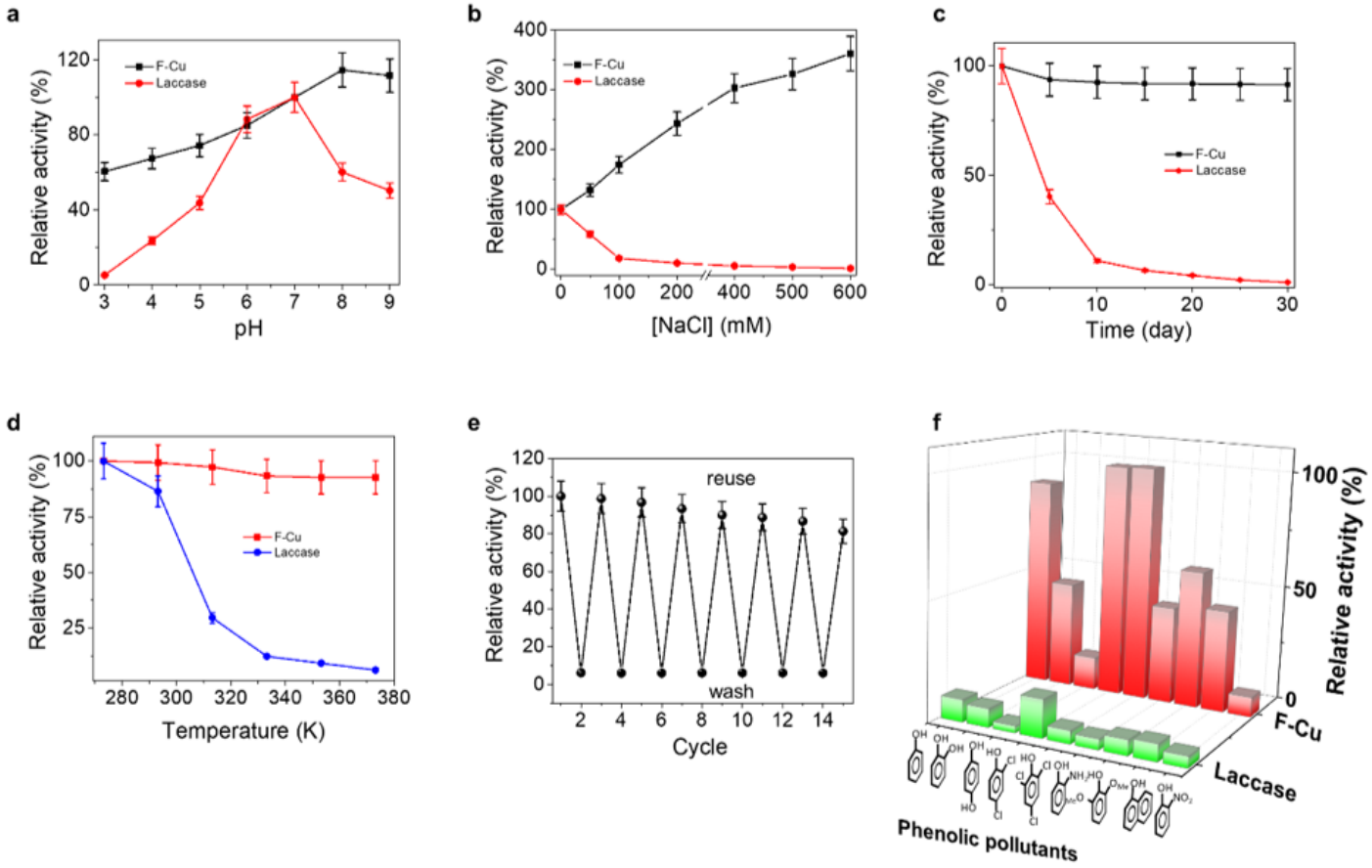

Figure 4

Catalytic stability, reusability, and substrate universality of F-Cu bionanozyme. a-d, Relative activity of F-Cu and laccase under various (a) pH values, (b) ionic strength (NaCl concentration), (c) storage time, and (d) incubation temperature. e, Relative activity during the F−Cu recycling process (the condition for the recycling experiments: 0.1 mg/mL 2,4- DP, 0.1 mg/mL 4-AP, 0.1 mg/mL F-Cu, pH 7.25, 25 °C, 1 h). f, Relative catalytic conversion activity of the F-Cu bionanozyme and laccase for various toxic phenolic pollutants.

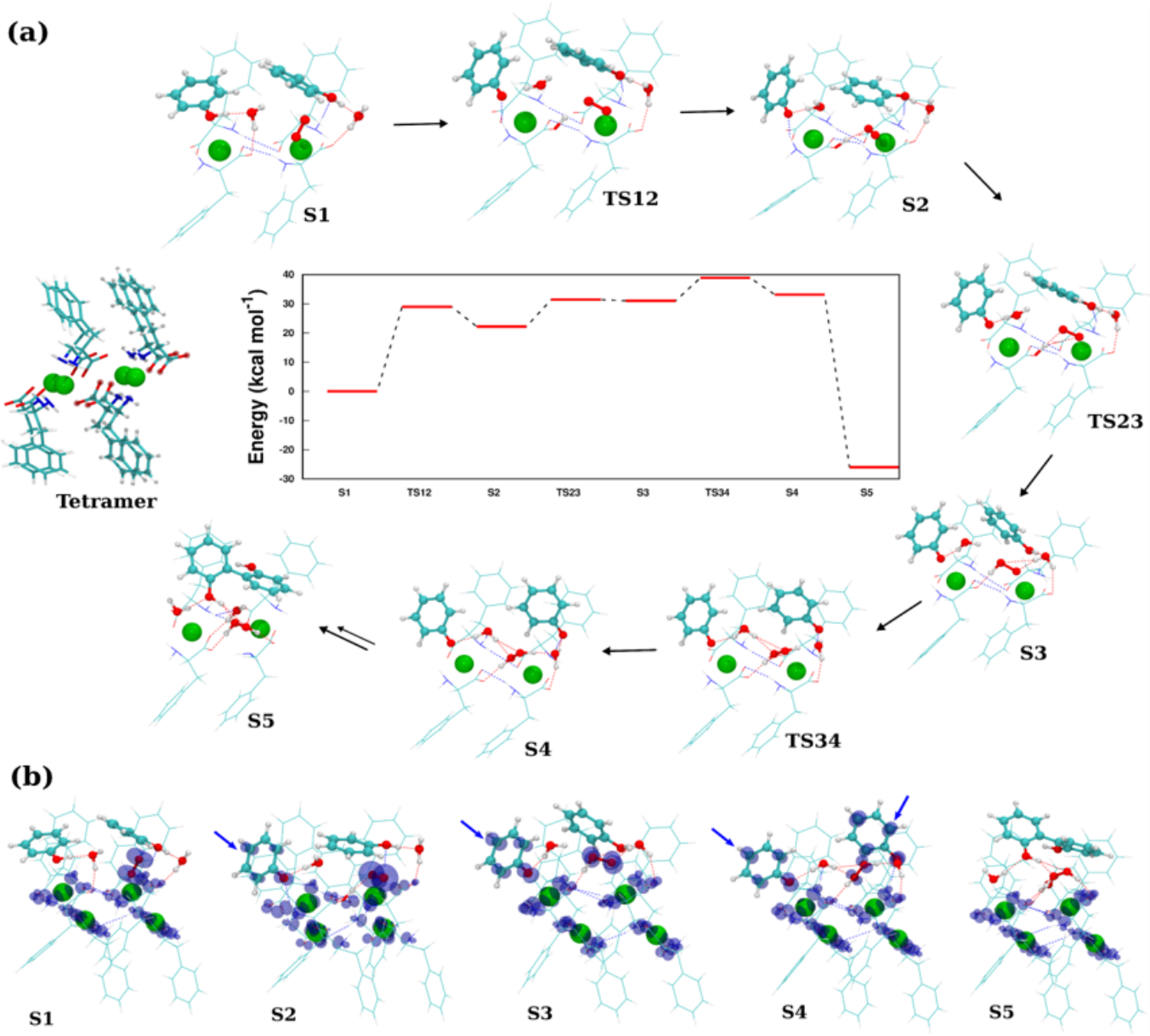

Figure 5

Reaction pathway for F–Cu catalytic oxidative coupling of phenolic pollutants. a, The tetramer model of F-Cu used in the simulations are shown on the left. The atoms displayed as transparent beads in the tetramer were held fixed throughout the calculations to emulate periodic crystal effects. Relative energies of step 1 through 5 along with the transition state energies, scaled with respect to step 1, are shown in the central part of the panel. The optimized structures of all steps are also shown, where the fixed atoms are not shown for clarity. b, Spin-densities of step 1 through 5. Spin-densities on the phenyl rings of the phenoxyl radicals are indicated by the blue arrows.

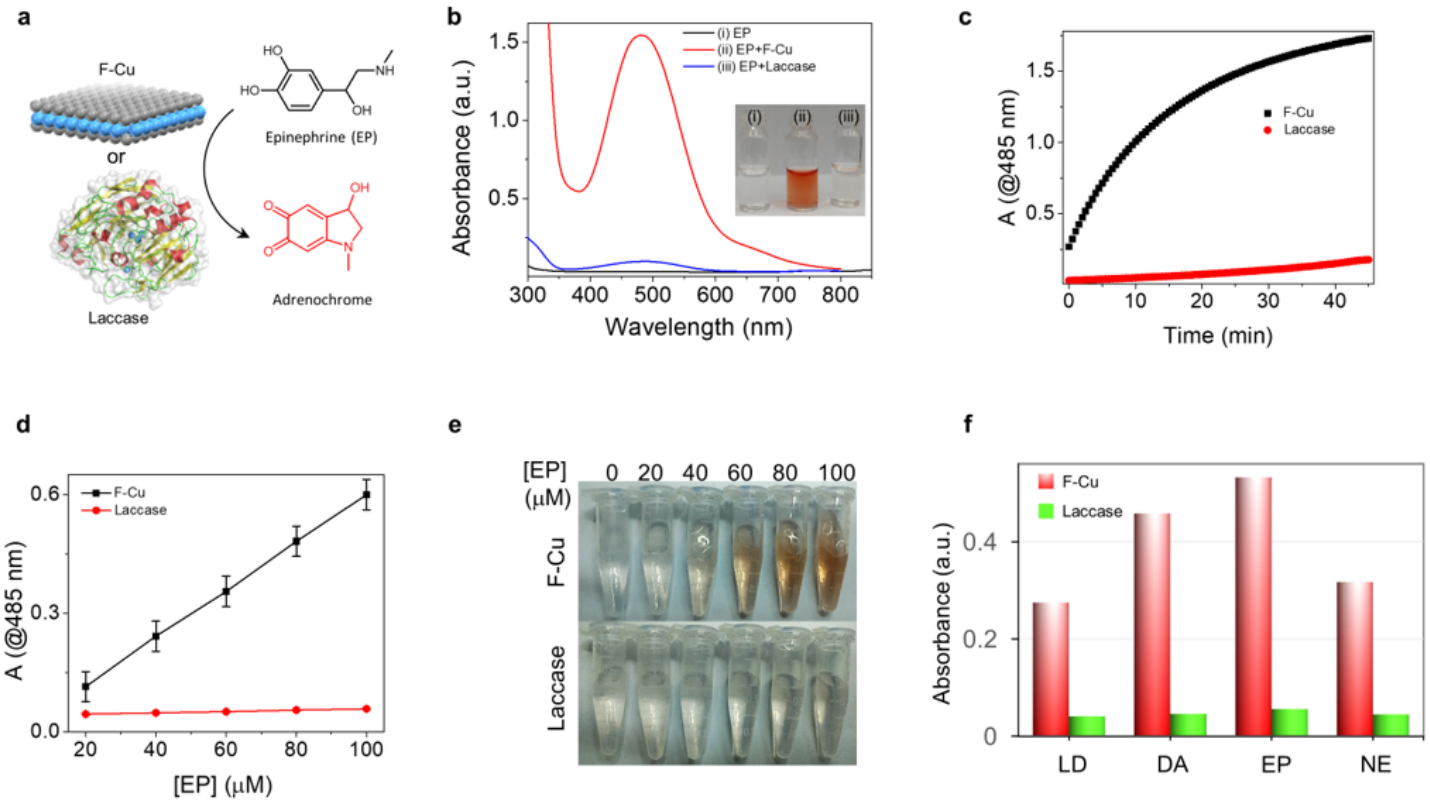

Figure 6

Colorimetric detection of catecholamine neurotransmitters. a, Schematic reaction illustration of colorless epinephrine (EP) oxidation reaction into the chromogenic product catalyzed by F-Cu or laccase. b, UV–vis spectra of (i) EP as well as its oxidation product catalyzed by (ii) F-Cu and (iii) laccase. c, Comparison of the progress of epinephrine oxidation reaction catalyzed by F-Cu and laccase. d, Linear relationships between the absorbance at 485 nm and the concentration of EP in the presence of F-Cu and laccase. e, Photographs of visible detection of different concentrations (5–30 μg/mL) of EP. f, Comparison of the relative activity of F-Cu and laccase catalyzing the oxidation of four different catecholamine neurotransmitters substrates, L-DOPA (LD), dopamine (DA), epinephrine (EP), and norepinephrine (NE).

Supplementary Files

This is a list of supplementary files associated with this preprint. Click to download.

- SI.docx
- MovieS1.mp4
- MovieS2.mp4
- MovieS3.mp4
- MovieS4.mp4

- graphicalabstract.png